Sensitivities of Summertime Mesoscale Circulations in the Coastal Carolinas to Modifications of the Kain–Fritsch Cumulus Parameterization

AARON P. SIMS

State Climate Office of North Carolina, Department of Marine, Earth, and Atmospheric Sciences, North Carolina State University, Raleigh, North Carolina

KIRAN ALAPATY

Systems Exposure Division, National Exposure Research Laboratory, U.S. Environmental Protection Agency, Research Triangle Park, North Carolina

SETHU RAMAN

Department of Marine, Earth, and Atmospheric Sciences, North Carolina State University, Raleigh, North Carolina

(Manuscript received 4 February 2016, in final form 22 August 2017)

ABSTRACT

Two mesoscale circulations, the Sandhills circulation and the sea breeze, influence the initiation of deep convection over the Sandhills and the coast in the Carolinas during the summer months. The interaction of these two circulations causes additional convection in this coastal region. Accurate representation of mesoscale convection is difficult as numerical models have problems with the prediction of the timing, amount, and location of precipitation. To address this issue, the authors have incorporated modifications to the Kain–Fritsch (KF) convective parameterization scheme and evaluated these mesoscale interactions using a high-resolution numerical model. The modifications include changes to the subgrid-scale cloud formulation, the convective turnover time scale, and the formulation of the updraft entrainment rates. The use of a grid-scaling adjustment parameter modulates the impact of the KF scheme as a function of the horizontal grid spacing used in a simulation. Results indicate that the impact of this modified cumulus parameterization scheme is more effective on domains with coarser grid sizes. Other results include a decrease in surface and near-surface temperatures in areas of deep convection (due to the inclusion of the effects of subgrid-scale clouds on the radiation), improvement in the timing of convection, and an increase in the strength of deep convection.

1. Introduction

Summertime convective precipitation in the coastal Carolinas is often forced by two important mesoscale processes (Raman et al. 2005). These two mechanisms are the deep convection that develops over the Sandhills and the sea-breeze circulation. The Sandhills is a sandy land surface, oriented parallel to the coast, and adjacent to clay soils (Fig. 1). For comparable water content, the thermal diffusivity for sandy soil is higher than clay soil (Arya 2001) allowing the Sandhills to heat faster than the surrounding regions. This thermal gradient can initiate surface convergence and cumulus convection. Deep convection over the Sandhills produces cool downdrafts resulting in a shallow density current, ''the Sandhills front,'' which interacts with the sea-breeze front. Interaction of these two fronts produces strong vertical motion and additional convection and precipitation (Sims and Raman 2016).

The skill of numerical models to forecast locally driven convective summertime precipitation is poor relative to other advancements in numerical weather prediction (Fritsch and Carbone 2004; Cao and Zhang 2016). At coarser grid spacing (>4 km), cumulus parameterization schemes help to address unresolved finer-scale convective events. However, convective parameterizations often overpredict the areal extent and amounts of precipitation (Liu et al. 2006; Clark et al. 2007; Yu and Lee 2010). Models that use these schemes tend to overpredict the frequency of precipitation events and underpredict amounts in heavier ones (Janowiak et al. 2007). In the Southeast United States, which

Corresponding author: Aaron Sims, apsims@ncsu.edu

DOI: 10.1175/MWR-D-16-0047.1

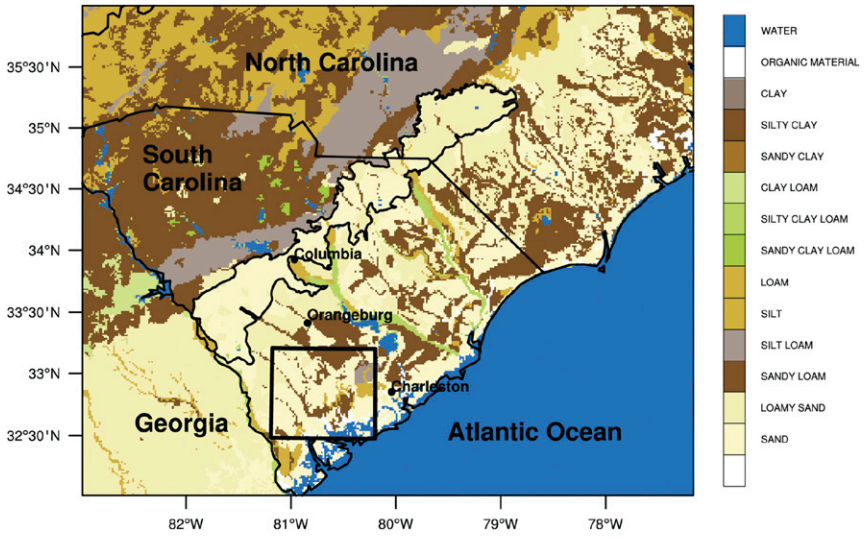

FIG. 1. Dominant soil-type categories for the Carolinas. The Carolina Sandhills area extends from southern North Carolina through central South Carolina and is outlined in black. The black box encompasses the region of mesoscale interaction between the sea-breeze front and the Sandhills front for the case studies presented in this paper.

includes the coastal Carolinas, these models also tend to initiate convection earlier than observed in the afternoon (Janowiak et al. 2007; Lee et al. 2007; Choi et al. 2015).

Grid spacing is an important factor to consider when simulating mesoscale-driven precipitation events. Grids using higher resolutions tend to simulate precipitation maximums better (Clark et al. 2009). For weak synoptic forcing, it has been suggested that subkilometer scales are required to adequately predict mesoscale events (Liu et al. 2006). Until recently, numerical simulations at resolutions fine enough to eliminate the need for a cumulus parameterization were prohibitively computationally expensive. Additionally, many microphysics schemes tend to produce excessive precipitation (Blossey et al. 2007). Until large uncertainties present in cloud microphysics (Cintineo et al. 2014) are reduced, cumulus parameterizations are still needed, particularly at coarser grid resolutions.

The Kain–Fritsch (KF) cumulus parameterization (CP) scheme is widely used in numerical models and performs reasonably well in the Southeast United States (e.g., Wang and Seaman 1997; Liang et al. 2004). This CP scheme is a mass flux parameterization characterized by three distinct parts: a trigger mechanism to determine if convection will occur, a mass flux formulation of the entrainment/detrainment plume model, and a CAPE closure assumption (Kain and Fritsch 1990, 1993; Kain 2004). Modifications to the Kain–Fritsch scheme presented in this paper have been used earlier in air quality and regional climate simulations (Alapaty et al. 2012; Herwehe et al. 2014a; Bullock et al. 2015) and to simulate synoptically driven events in the Midwest United States (Zheng et al. 2016). However, applications to mesoscale, locally driven convective events have not been evaluated.

In this study, we explore the efficacy of these KF CP modifications on the prediction of summertime convective precipitation over the Carolinas. The objectives of this study are to explore the effects of the modified KF CP scheme on 1) the mitigation of overprediction of precipitation at high resolutions, 2) the timing of convection initiation for these mesoscale interaction events, and 3) the predictability of precipitation from locally driven convection at high resolutions. This paper is arranged in the following manner. The modifications to the KF CP scheme are presented in section 2. The design of the numerical simulations is described in section 3. Sections 4 and 5 evaluate the performance of the KF CP scheme using two separate case studies, followed by the summary and conclusions in section 6.

2. Kain–Fritsch modifications

Modifications to the Kain–Fritsch scheme include adjustments to the cloud fraction (Alapaty et al. 2012, 2014a), changes to the convective turnover time scale, and improvements to the entrainment formulations (Zheng et al. 2016). The updated Kain–Fritsch (UKF) parameterization also incorporates a grid-aware scaling parameter into these modifications. An evaluation of the contributions of the individual modifications is

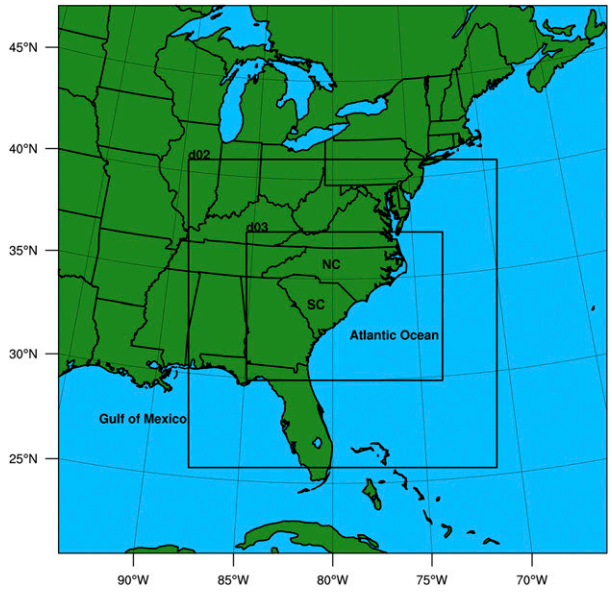

FIG. 2. Simulated domains centered over the Carolinas. North Carolina is indicated by NC and South Carolina is indicated by SC. The outermost domain has a grid spacing of 12 km, the middle domain (d02) is 4 km, and the inner domain (d03) is 1 km.

presented in Herwehe et al. (2014b). They used 3-month summer seasonal simulations at 12-km grid spacing over the eastern two-thirds of the continental United States for evaluation of the CP scheme. Their results indicate that the individual and cumulative effects of changes to the KF CP scheme improve the forecasts of precipitation, cloudiness, radiation, and air temperature. For clarity and completeness, each of these modifications to the CP scheme is described herein.

a. Subgrid-scale clouds

Modifications to the KF subgrid-scale cloudiness follow the methods of Xu and Krueger (1991) where the net cloud fraction is incorporated into the Rapid Radiative Transfer Model for GCMs (RRTMG) shortwave and longwave radiation schemes (Iacono et al. 2008). The KF scheme uses in-cloud updraft mass fluxes at each vertical level to estimate convective cloud fraction, and then adjusts the resolved cloud fraction. The grid-scale cloud fraction is determined by the relative humidity in the grid volume.

The subgrid-scale cloud fraction, CLDFRAC, adjusts the grid-scale cloud fraction, CLDFRAG, by the following formulation:

$$\text{ACLDFRAG} = (1 - \text{CLDFRAC})\text{CLDFRAG}, \quad (1)$$

where the adjusted grid-scale cloud fraction is ACLDFRAG. The new total cloud fraction is the sum of the adjusted grid-scale cloud fraction and the one estimated by the cumulus parameterization scheme. These modifications have been incorporated into v3.6 and newer versions of the WRF Model (Skamarock and Klemp 2008).

TABLE 1. Model features.

Domain	12 km	4 km	1 km
CP scheme (CONTROL)	KF	None	None
CP scheme (ALLCU)	KF	KF	KF
CP scheme (UKF)	UKF	UKF	UKF
PBL scheme	MYNN2.5	MYNN2.5	MYNN2.5
LSM	Noah	Noah	Noah
Microphysics	WSM6	WSM6	WSM6
Radiation	RRTMG	RRTMG	RRTMG
Initialization and boundary conditions	GFS analysis	GFS analysis	GFS analysis
Horizontal grid	250 × 250	421 × 421	1069 × 809
Vertical levels	51	51	51

b. Convective time scale

Dating back to Fritsch et al. (1976) and Fritsch and Chappell (1980), the convective time step τ has been proportional to the grid length DX, and thus connected to the advective time scale of clouds. This convective time-scale formulation was developed at grid lengths of 20–25 km and is related to the time it takes a cloud to be advected through a grid box by the mean wind. This relationship between grid length and the convective time step is still in practice today even as grid lengths have decreased well below 20 km.

The convective time scale in the Kain–Fritsch CP scheme is based on stability restoration time for a given amount of convective available potential energy (CAPE) (Kain and Fritsch 1993). In general, the amount of CAPE is independent of the grid spacing. Under the current KF CP formulation, when the grid spacing decreases, the convective time scale stays at a minimum prescribed value of 1800 s. With this value, the updrafts and consequent precipitation amounts will be unrealistically intense at fine grid resolutions (Bullock et al. 2015). Also, as grid lengths decrease, the convection will be resolved by grid-scale microphysics. Currently, the grid resolution at which the CP scheme is turned off is subjective.

To address these deficiencies, the UKF CP scheme is designed to ramp down its influence at higher resolutions in a systematic physical manner by reformulating the convective turnover time scale τ (s). This formulation of τ, is based on a relationship for the convective velocity derived by Grant and Lock (2004), a relation for convective time scale by Bechtold et al. (2008), and a scaling parameter adjustment as a function of the grid

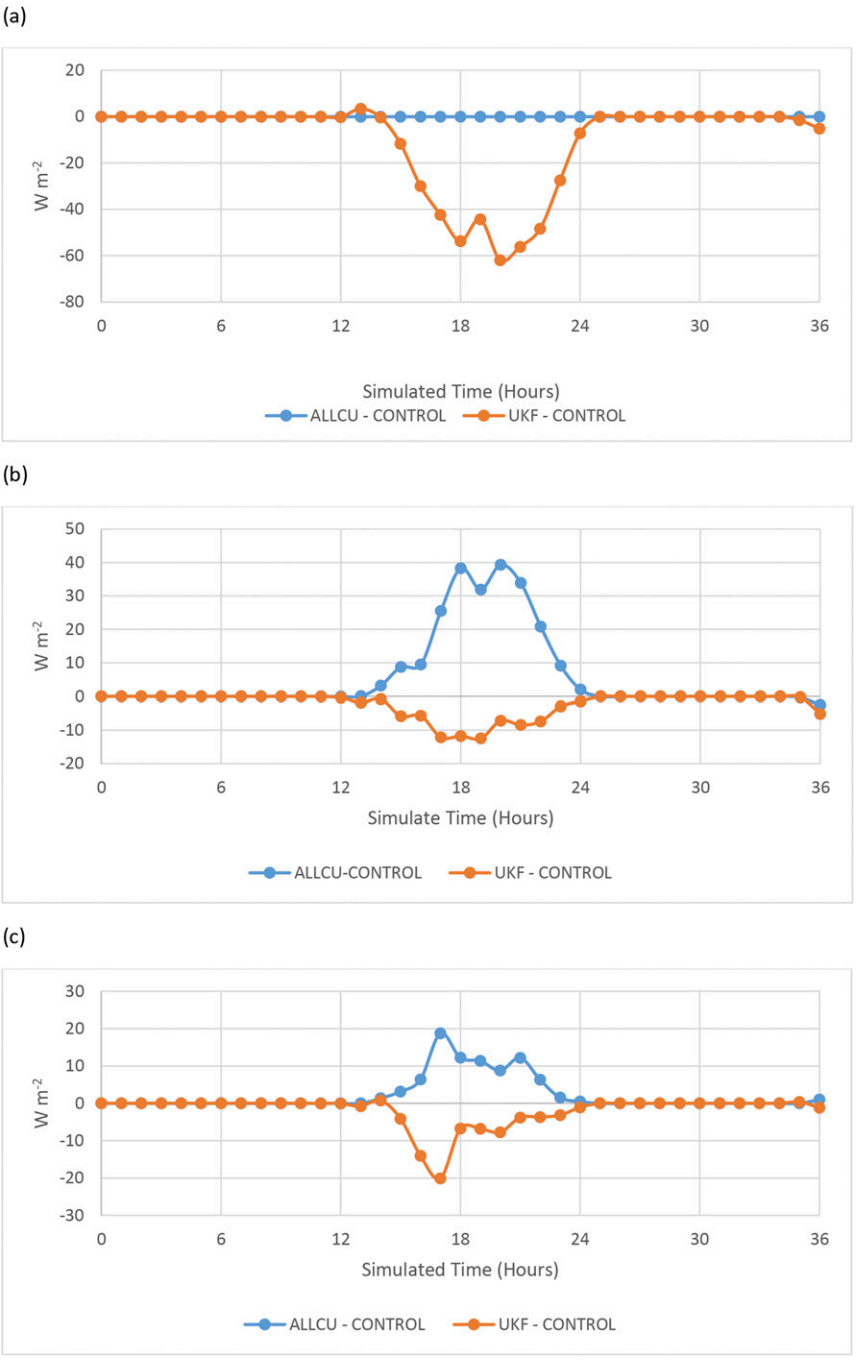

FIG. 3. Differences in downward shortwave radiation for each simulation from the CONTROL simulation. Zero hour corresponds to 0000 UTC 24 Jun 2009: (a) 12-, (b) 4-, and (c) 1-km grid-averaged differences.

resolution introduced by Alapaty et al. (2014b). This time scale is given by the following relation:

$$\tau = \frac{H}{(\delta m_b A_e)^{1/3}}\beta, \tag{2}$$

where H is the cloud depth in meters, δm_b is the cloud-base updraft mass flux per unit density (in $\mathrm{m\,s^{-1}}$), A_e is the potential energy of the saturated air supplied to the cloud base (in $\mathrm{m^2\,s^{-2}}$), and β is the scaling parameter defined as

$$\beta = 1 + \ln(25/DX), \tag{3}$$

where DX is the grid size (km).

Essentially, the convective turnover time scale τ is related to the number of updrafts needed to reduce the CAPE by the prescribed 90%. Small values of τ lead to intense updrafts and, hence, intense convection. As grid spacing decreases, atmospheric stability restoration is performed by the grid-scale cloud microphysics scheme; thus, the subgrid-scale convection tendencies must decrease. Ideally at cloud-resolving scales, subgrid-scale tendencies should vanish completely. This functionality of τ is achieved by utilizing the scaling parameter β, which is analogous to the findings of a cloud-resolving modeling study by Arakawa and Wu (2013). They showed that the resolved cloud fraction will vary in a bimodal fashion as grid spacing is reduced from that of a coarse general circulation model to a fine cloud-resolving model.

Traditionally, the convective turnover time scale affects precipitation amounts inversely. Smaller time scales allow more precipitation to fall within the air column before the cloud is advected out of the grid cell. In the new dynamic τ formulation, as the grid spacing decreases, τ increases. This allows the UKF CP scheme to continue to be active at higher resolutions. Longer convective time scales do not stabilize the atmosphere as quickly, reducing excessive precipitation and allowing moisture to be retained in the atmosphere. To help facilitate grid-scale saturation, the convective updraft mass flux is converted into updraft vertical velocity, which in turn enhances the grid-scale vertical velocity (Zheng et al. 2016). These UKF updates are now available in the multiscale Kain–Fritsch scheme (Alapaty et al. 2014a).

c. *Entrainment*

Entrainment in the KF CP scheme is loosely dependent on the cloud radius and the mean grid-resolved vertical velocity at the cloud base. The cloud radius dependency in the entrainment formulation is somewhat arbitrary, creating a dependency of convection initiation on larger-scale forcing (Kain 2004). As grid spacing decreases, the prescribed fixed cloud radius causes grid-box saturation. To address this deficiency, the dynamic entrainment formulation (Zheng et al. 2016) follows a similar concept as the dynamic τ formulation. Utilizing the scaling parameter β, the mixing rate is defined by

$$\Delta M_e = M_b \frac{\alpha\beta}{z_{\mathrm{LCL}}} \Delta p, \tag{4}$$

where $\alpha = 0.03\,\mathrm{m\,Pa^{-1}}$ is a constant of proportionality (Kain 2004), M_b is the updraft mass flux per unit area ($\mathrm{kg\,s^{-1}}$) at the cloud base, β is the scaling parameter [Eq. (3)], Δp is the pressure depth of a model level, and z_{LCL} (m) is the height of the cloud base. The height of the cloud base replaces the arbitrary fixed cloud radius since entrainment is a function of subcloud layer depth. As the product $\alpha\beta$ increases, the mixing rate will increase (Tokioka et al. 1988; Kim et al. 2009), thus limiting subgrid convection, particularly in drier environments (Lin et al. 2013).

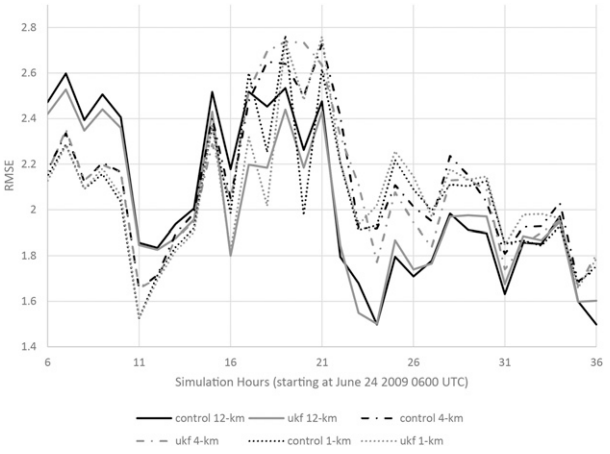

FIG. 4. A time series of area-averaged root-mean-square error of the 2-m air temperature (°C) using hourly observations in SC. The black lines represent the CONTROL simulation with the solid line for the 12-km domain, the dot–dashed line for the 4-km domain, and the dotted line representing the 1-km domain. The gray lines indicate the UKF simulations following the same line style pattern for each domain.

This new scale-aware entrainment formulation allows the mixing rate, ΔM_e, to increase with decreasing grid spacing DX. At higher resolutions, the effects of the KF CP scheme are reduced, inhibiting deep convection. Increased entrainment associated with decreased grid spacing has been simulated in several large-eddy simulations and cloud-resolving modeling studies (e.g., Stevens and Bretherton 1999; Del Genio and Wu 2010; Romps and Kuang 2010; Bryan and Morrison 2012).

3. Model configuration

Two different cases of mesoscale convective events are simulated using the Weather Research and Forecasting (WRF) Model (version 3.3.1). Three simulation domains are used (Fig. 2). The outermost, intermediate, and inner domain grid spacings are 12, 4, and 1 km, respectively. Both cases use one-way nesting with the innermost domain centered over the Carolinas region. Each simulation is performed for 36 h and is initialized at 0000 UTC on the day of the convective event, giving ample spinup time before the development of convection in the region. Physics options, grid dimensions, initialization, and boundary conditions used in the simulations are shown in Table 1.

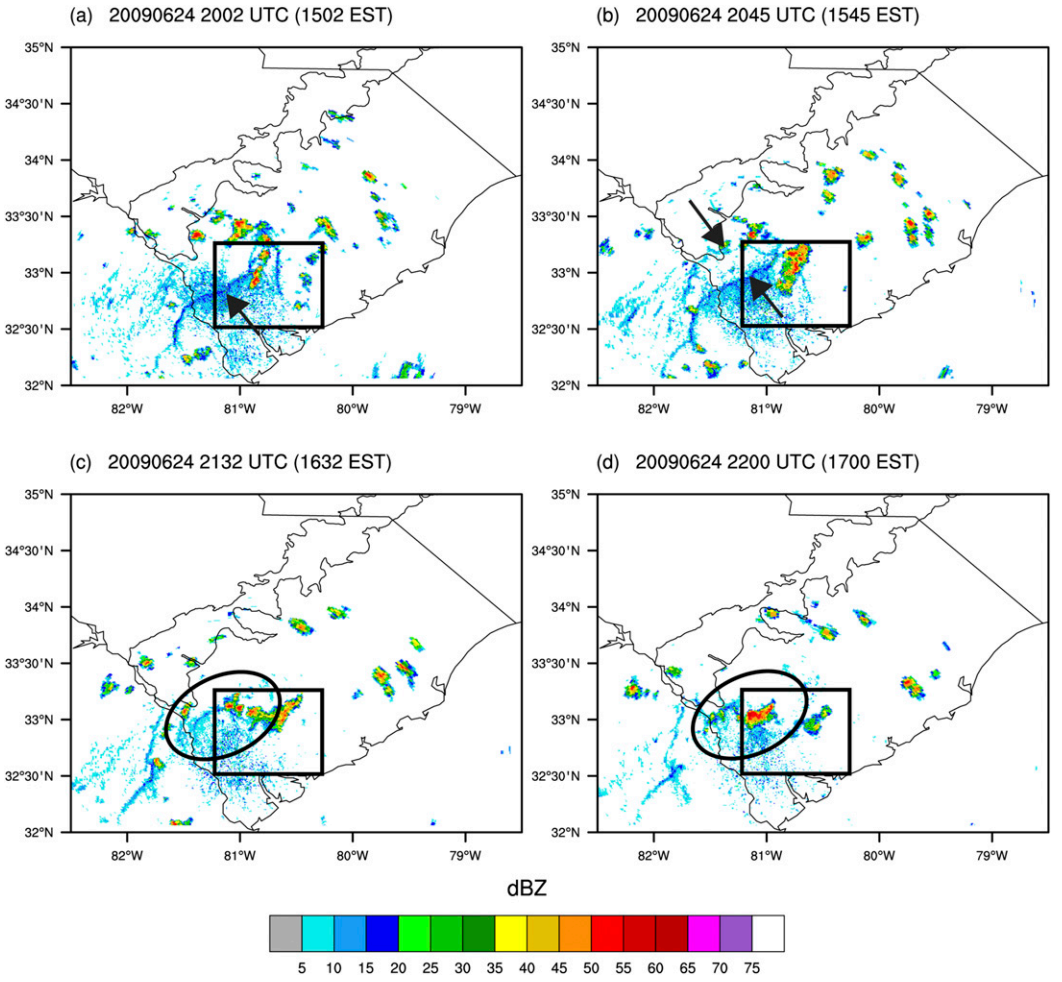

FIG. 5. Snapshots in time of the base-level radar reflectivity (dBZ) from the Doppler radar in Charleston, SC, on 24 Jun 2009. The black box indicates the study area (Fig. 1). (a) The sea-breeze front is indicated by the black arrow and the thin blue line of reflectivity at 2002 UTC. (b) The development of the Sandhills front from the outflow of convection in the Sandhills at 2045 UTC (fronts indicated by opposing arrows). (c) Merging of the sea-breeze front and the Sandhills front at 2132 UTC (circled area). (d) Convection in southern SC at 2200 UTC where the Sandhills front and the sea-breeze front merged.

Each case study, one on 24 June 2009 (case 1) and the other on 27 June 2010 (case 2), has a simulation designated as CONTROL with the KF CP scheme deployed only on the 12-km domain. The second simulation, UKF, for each case study incorporates the KF CP modifications on all domains. For case 1, a simulation designated as ALLCU uses the unmodified KF CP scheme on all domains (12, 4, and 1 km). It is used as a baseline for comparing to the other simulations since domains of 4 km or less typically do not use a CP scheme (Weisman et al. 1997; Yu and Lee 2010).

4. Case 1 simulation

Processes involved in the initiation of deep convection and the interaction of the sea-breeze and Sandhills fronts are simulated. The differences in the CONTROL, UKF, and ALLCU simulations are discussed in the following sections.

a. Effect of subgrid-scale clouds on radiation

To assess the impact of the daily cycle of clouds, the incoming solar radiation is used as a proxy for the cloud cover over the region, where low values indicate the presence of clouds. For the region over South Carolina, differences in the grid-averaged downward shortwave radiation from the CONTROL are apparent (Fig. 3). These differences are most obvious for the 12-km domain averages where the CP scheme is more active. The maximum difference in the 12-km domain for the UKF simulation is a 60 W m^{-2} reduction in downward shortwave radiation (Fig. 3a).

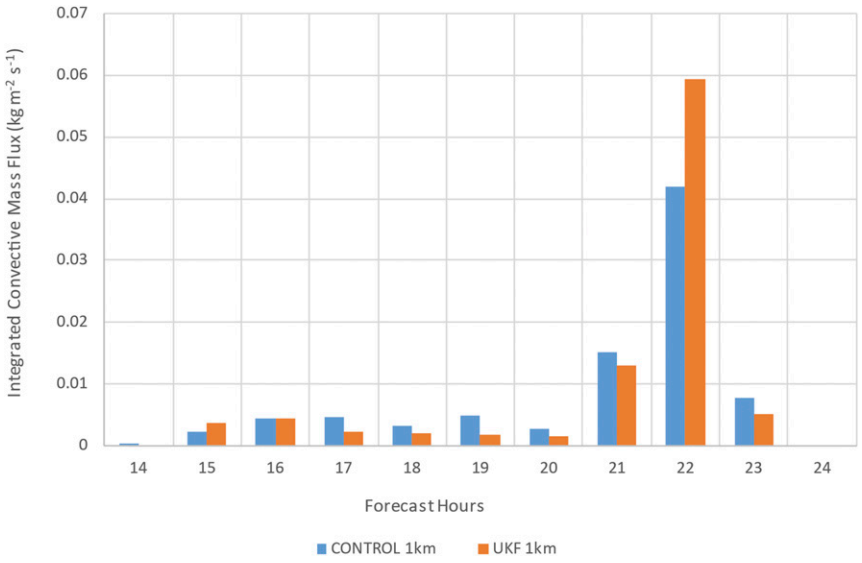

FIG. 6. Time history of convective mass flux (where $w > 2\,\mathrm{m\,s^{-1}}$ and $q_c + q_i > 0.005\,\mathrm{g\,kg^{-1}}$) in the region of interaction between the sea-breeze front and the Sandhills front during the afternoon of 24 Jun 2009 for the 1-km domain. The region of interaction is shown by the black box in Fig. 1. Forecast hours 14–24 correspond to times 1400 UTC 24 Jun–0000 UTC 25 Jun 2009.

The difference in the simulated incoming radiation is apparent at about 1400 UTC (0900 EST) 24 June 2009 and continues until near local sunset at 0100 UTC (2000 EST) 25 June 2009, corresponding to simulation hours 14–25.

In the 4-km domain, differences in the simulated radiation between the UKF and the CONTROL simulations are still evident but are of less magnitude, with a maximum difference of about $12\,\mathrm{W\,m^{-2}}$ that persists for several hours (Fig. 3b). Differences are largest during maximum daily heating (1700 UTC) and taper off toward sunset. The ALLCU simulation indicates higher radiation amounts at the surface than for the CONTROL, with a maximum difference of about $40\,\mathrm{W\,m^{-2}}$. Even in the 1-km domain (Fig. 3c), differences in the downward shortwave radiation between the simulations are apparent. These differences are most evident during peak heating. Incorporation of the subgrid-scale cloud processes in the UKF simulation causes a maximum decrease of $20\,\mathrm{W\,m^{-2}}$ in the incoming radiation. Thus, a discernible reduction in downward shortwave radiation in the UKF simulation is evident.

b. *Impacts on 2-m air temperature*

The impact of the modified radiation scheme on the simulated near-surface air temperatures over South Carolina is shown by the root-mean-square error (RMSE) in Fig. 4. The simulation grids are bilinearly interpolated to near-surface hourly observation locations. Each simulation hour in the graph uses an average of 45 stations. In the preconvective environment on 24 June 2009 (0600–1600 UTC), the simulated air temperatures in the two higher-resolution domains have less error. For most of the 36-h simulation, the UKF simulation (depicted by gray lines), has less air temperature errors than the CONTROL simulation (black lines) in the 12- and 1-km domains. The simulated air temperature in the UKF 4-km domain does not show improvement and has the highest temperature errors at peak daytime heating. The most notable improvement occurs in the outermost domain (12 km). The verifications at higher resolutions (4 and 1 km) are uncertain due to the double-penalty problem inherent in convective-scale forecasts (Gilleland et al. 2009). The incorrect placement of individual convective cells during the afternoon hours (1600–2200 UTC) can increase the RMSE of an otherwise accurate forecast.

c. *Development of convection*

Differences in the evolution of mesoscale convection between the CONTROL and the UKF simulations are demonstrated by evaluating the resolved upward convective cloud mass flux (UMF) following methods similar to Robe and Emanuel (1996) and Wang and Sobel (2011). The UMF at each vertical level is determined by including grid points in areas where the upward vertical

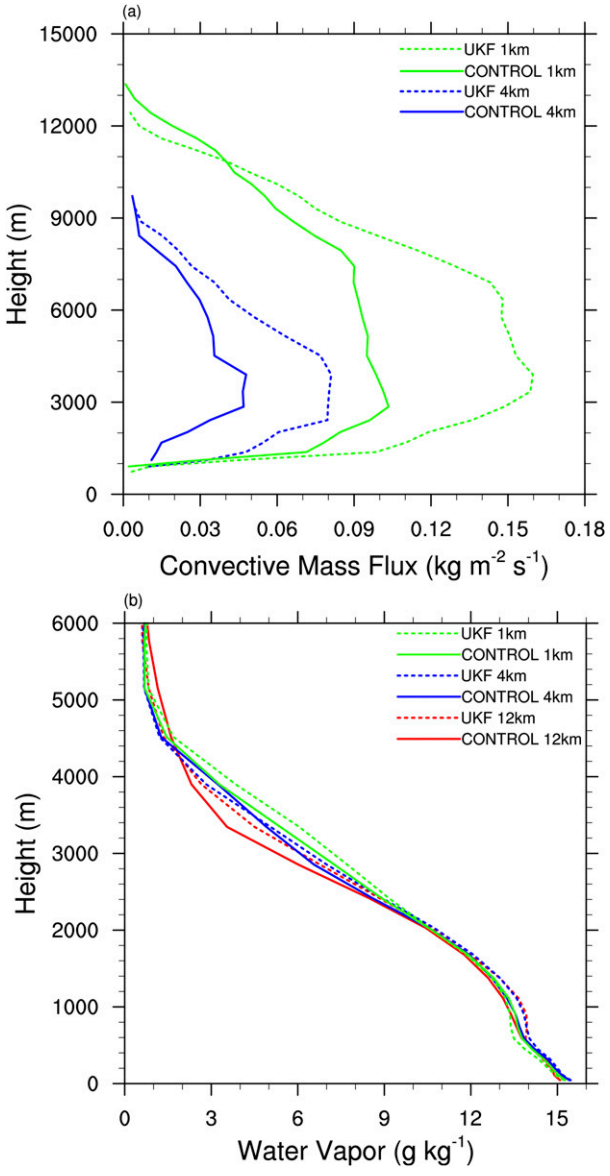

FIG. 7. Vertical profiles in the interaction region for the CONTROL and the UKF simulations for each of the domains at 2200 UTC 24 Jun 2009. Solid (dashed) lines represent the CONTROL (UKF) simulations. (a) Resolved convective mass flux ($\mathrm{kg\,m^{-2}\,s^{-1}}$). (b) Average water vapor mixing ratio ($\mathrm{g\,kg^{-1}}$).

velocity w exceeds $2\,\mathrm{m\,s^{-1}}$ and the total mixing ratio of cloud water q_c and ice q_i exceed $0.005\,\mathrm{g\,kg^{-1}}$. The grid-resolved UMF is given as

$$\mathrm{UMF} = \overline{\rho} A_c \frac{\sum w_{i,j}}{A}, \tag{5}$$

where $\overline{\rho}$ is the average density of the moist air, w is the vertical velocity, the subscripts i and j represent the indices on the horizontal grid, A_c is the area of a single grid box, and A is the total area of all the grid boxes. The area of mesoscale convection associated with the interaction between the Sandhills and sea-breeze fronts (Sims and Raman 2016) is indicated by the black box in Fig. 1.

Development of convection during the afternoon is shown by the base-level radar reflectivity from the Charleston, South Carolina, radar (Fig. 5). Location of the sea-breeze front is discernible as a thin line of radar reflectivity at 2002 UTC (Fig. 5a). Outflow from the convective storms in the Sandhills region can be seen at 2045 UTC by another thin line of radar reflectivity (Fig. 5b). The two mesoscale fronts are marked by opposing arrows. At 2132 UTC, convergence of these two fronts is observed, indicated by the black circle (Fig. 5c). Interaction of these two frontal features at 2200 UTC possibly causes additional convection (Fig. 5d).

A time history of UMF, in the region of interaction on 24 June 2009, is shown in Fig. 6. Throughout the afternoon, the UKF simulation predicts less convection than the CONTROL simulation as illustrated by the lower values of UMF. Increased convective turnover time scale from the updated KF CP scheme modulates the development of strong convection in early afternoon. During late afternoon, 2000–2200 UTC (forecast hours 20–22), when strong convection occurs (Fig. 5), the UKF simulation has larger values of UMF than the CONTROL simulation.

The vertical profile of UMF for the 1- and 4-km domains at 2200 UTC 24 June 2009 is shown in Fig. 7a. The grid-resolved values on the 12-km domain did not meet the criteria of $w > 2\,\mathrm{m\,s^{-1}}$ and $q_c + q_i > 0.005\,\mathrm{g\,kg^{-1}}$ and, hence, are not included. Each of the UKF-simulated domains has a higher UMF than the respective CONTROL domains of the same resolution. The UMF profiles indicate that the convective mass flux rapidly increases in the boundary layer with the highest values in the lower to midtroposphere. The 1-km domain in the UKF simulation has a maximum UMF of $0.16\,\mathrm{kg\,m^{-2}\,s^{-1}}$ at a height of 4000 m. The 1-km domain in the CONTROL simulation has a maximum value of $0.10\,\mathrm{kg\,m^{-2}\,s^{-1}}$ at a height of 3000 m. Overall, the UKF simulation predicts stronger and deeper convection in the interaction area than the CONTROL simulation.

Vertical profiles of average water vapor mixing ratio in the interaction area at 2200 UTC 24 June 2009 for the CONTROL and UKF simulations are shown in Fig. 7b. There are larger values of specific humidity in the UKF simulation between heights of 1 and 4 km. These differences could be due to the modifications made to the entrainment and a larger convective time step. The scaling parameter in the UKF simulation slows the ability of the CP scheme to overturn the atmosphere and remove the CAPE and moisture. The entrainment rates are also

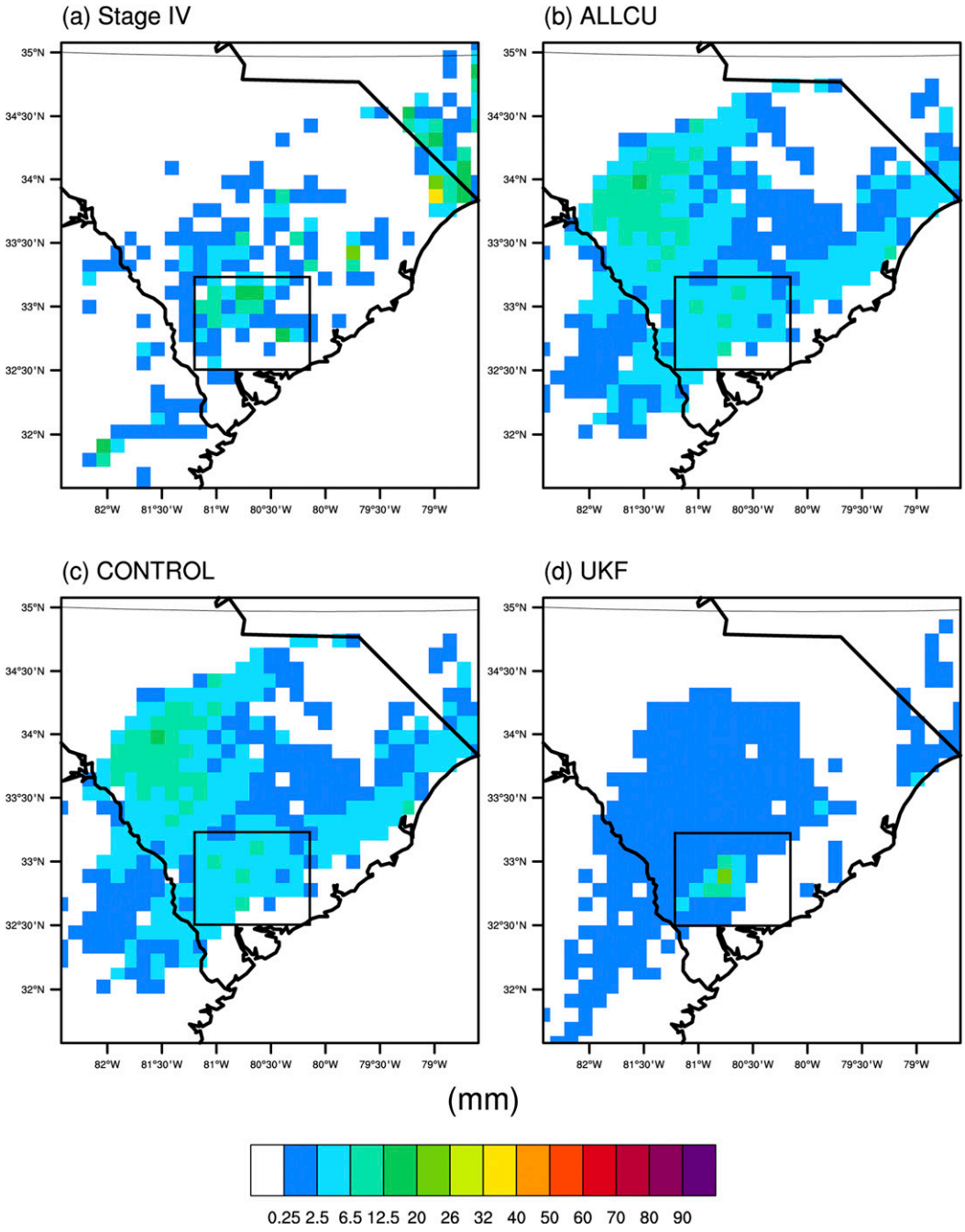

FIG. 8. Total accumulated precipitation (mm) centered over South Carolina for the period 0000 UTC 24 Jun–1200 UTC 25 Jun 2009. The black box indicates the study area, depicted in Fig. 1. (a) Stage-IV analyses regridded to the 12-km WRF domain. (b) Predicted precipitation amounts from the 12-km ALLCU simulation. (c) Predicted precipitation amounts from the 12-km CONTROL simulation. (d) Predicted precipitation amounts from the 12-km UKF simulation.

higher at finer grid scales, diminishing the effect of the CP scheme. The reduced consumption of moisture and CAPE by the CP scheme can result in more intense deep convection induced by the grid-scale microphysics scheme.

d. Total precipitation

The total precipitation from the 36-h simulations is compared to the Stage-IV Multisensor Precipitation Estimates (Stage-IV analyses) obtained from the National

TABLE 2. Frequency bias (FBIAS) and mean error (ME) for total precipitation (mm) for the 24 Jun 2009 case over the South Carolina region for each simulation.

Statistic	Threshold	CONTROL 12 km	UKF 12 km	CONTROL 4 km	UKF 4 km	CONTROL 1 km	UKF 1 km
FBIAS	≥0.254	1.571	1.311	1.369	1.421	1.386	1.497
FBIAS	≥1.270	2.596	1.088	1.655	1.583	1.721	1.751
FBIAS	≥2.540	3.216	0.270	1.811	1.647	1.921	1.921
FBIAS	≥6.350	1.000	0.267	2.122	1.891	2.116	2.220
FBIAS	≥12.700	0.000	0.250	4.485	4.121	4.246	4.886
ME		0.928	−0.362	1.332	1.279	1.301	1.450

Centers for Environmental Prediction (NCEP). Stage-IV analyses are created by calibrating the radar-derived estimated precipitation amounts with observed precipitation from rain gauges. These gauge-calibrated radar estimates undergo a level of human quality control at the River Forecast Centers, and are mosaicked together onto a national 4.765-km grid by NCEP (Lin and Mitchell 2005). The spatial resolution and 6-h time frequency makes Stage-IV analyses unique and valuable for evaluating precipitation patterns. However, Stage-IV precipitation analyses have some limitations. These limitations include inherent biases, particularly in locally driven convective events. Stage-IV analyses also tend to underestimate the heaviest precipitation and overestimate the lower precipitation amounts (Habib et al. 2009; Wootten and Boyles 2014). Inaccuracies in Stage-IV analyses provide an additional source of uncertainty, particularly when comparing these data on a 1-km domain. Even with these errors, Stage-IV analyses are still very useful for evaluating the spatial distributions and amounts of precipitation simulated by numerical models.

The total simulated precipitation is evaluated using Stage-IV analyses at different thresholds. Frequency bias (FBIAS) is used to quantify the ratio of the total number of events forecasted to the total number of observations where

$$\text{FBIAS} = \frac{\sum \eta_{11} + \sum \eta_{10}}{\sum \eta_{11} + \sum \eta_{01}}. \tag{6}$$

The subscripts of η represent an occurrence or nonoccurrence of an event. The first and the second subscripts represent the model and the observations, respectively. A value of one for the model indicates precipitation was predicted, while a value of zero indicates it was not. Similarly, a value of one (zero) for the observations indicates precipitation occurred (did not occur). A FBIAS of one indicates the occurrence of the same number of forecasted and observed events. Values greater than one indicate too many locations were forecasted to have precipitation (too wet), and values less than one indicate not enough locations were forecasted (too dry).

The mean error (ME) is used to evaluate the overall precipitation bias and is obtained using the relation,

$$\text{ME} = \frac{1}{n}\sum f_i - o_i, \tag{7}$$

where f_i represents the forecast values, o_i is the observed values, and n is the total number of values. A perfect forecast has a ME equal to zero (no bias). Negative (positive) values indicate that the average simulation values are smaller (larger) than the observations.

The 36-h total precipitation from Stage-IV analyses for the period 0000 UTC 24 June–1200 UTC 25 June 2009 are regridded to the 12-km simulation domain (Fig. 8a). Stage-IV analyses are not shown over water where there are no precipitation gauges available to improve its accuracy. Stage-IV analyses indicate that most of the precipitation occurred in the coastal plains of South Carolina with localized maxima. In southern South Carolina near the coast, precipitation amounts of up to 12.5 mm occur in the area of interest, the area of interaction between the sea-breeze front and the Sandhills front (Sims and Raman 2016).

The 12-km ALLCU and CONTROL simulated precipitation fields (Figs. 8b and 8c) are identical since both domains are configured using the same physics. The CONTROL simulation overpredicts the spatial extent of the precipitation and has a different location for maximum precipitation than Stage-IV analyses (Fig. 8a). Precipitation from the CONTROL simulation covers too large areal extent in South Carolina with the highest amounts, 12.5–20.0 mm, occurring in central South Carolina. Central South Carolina was not the location of the observed maximum precipitation; Stage-IV analyses indicate little to no precipitation in central South Carolina. In contrast, there is much less total precipitation from the UKF simulation than in the CONTROL (Fig. 8d), reducing the overprediction of precipitation. Also, the precipitation maxima from UKF are more consistent with the observed Stage-IV analyses. However, there are locations (Fig. 8) where the scheme underpredicts the Stage-IV analyses amounts.

Frequency bias and mean error of the precipitation for the 12-km domain are shown in Table 2. The UKF

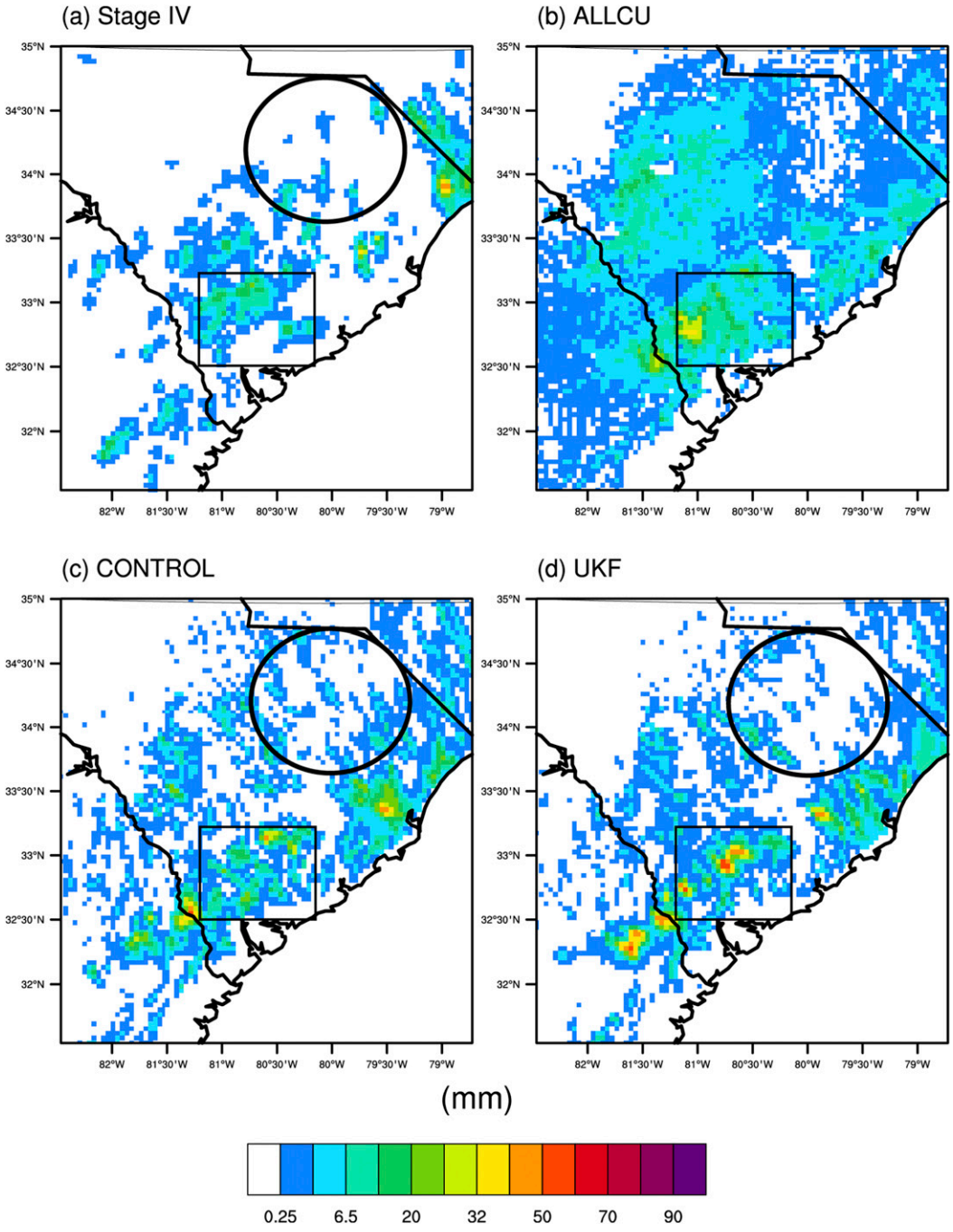

FIG. 9. As in Fig. 8, but for the 4-km domain. The black circle indicates an area where the UKF simulation agrees better with the Stage-IV analyses precipitation estimates than the CONTROL simulation.

simulation is less biased than the CONTROL simulation for smaller precipitation thresholds (<2.54 mm) with the FBIAS closer to 1. For amounts exceeding 2.54 mm, the CONTROL simulation has a FBIAS of over 3.2, while the UKF simulation is too dry with a FBIAS value of 0.27. At amounts greater than 6.35 mm the CONTROL simulation has a reduced FBIAS, outperforming the UKF simulation. However, the UKF simulation does mitigate the overprediction of precipitation seen in the CONTROL simulation, as indicated by the reduced bias (ME) in Table 2. The UKF simulation underpredicts the average amount by 0.362 mm, and the CONTROL simulation overpredicts precipitation with a ME of 0.928 mm.

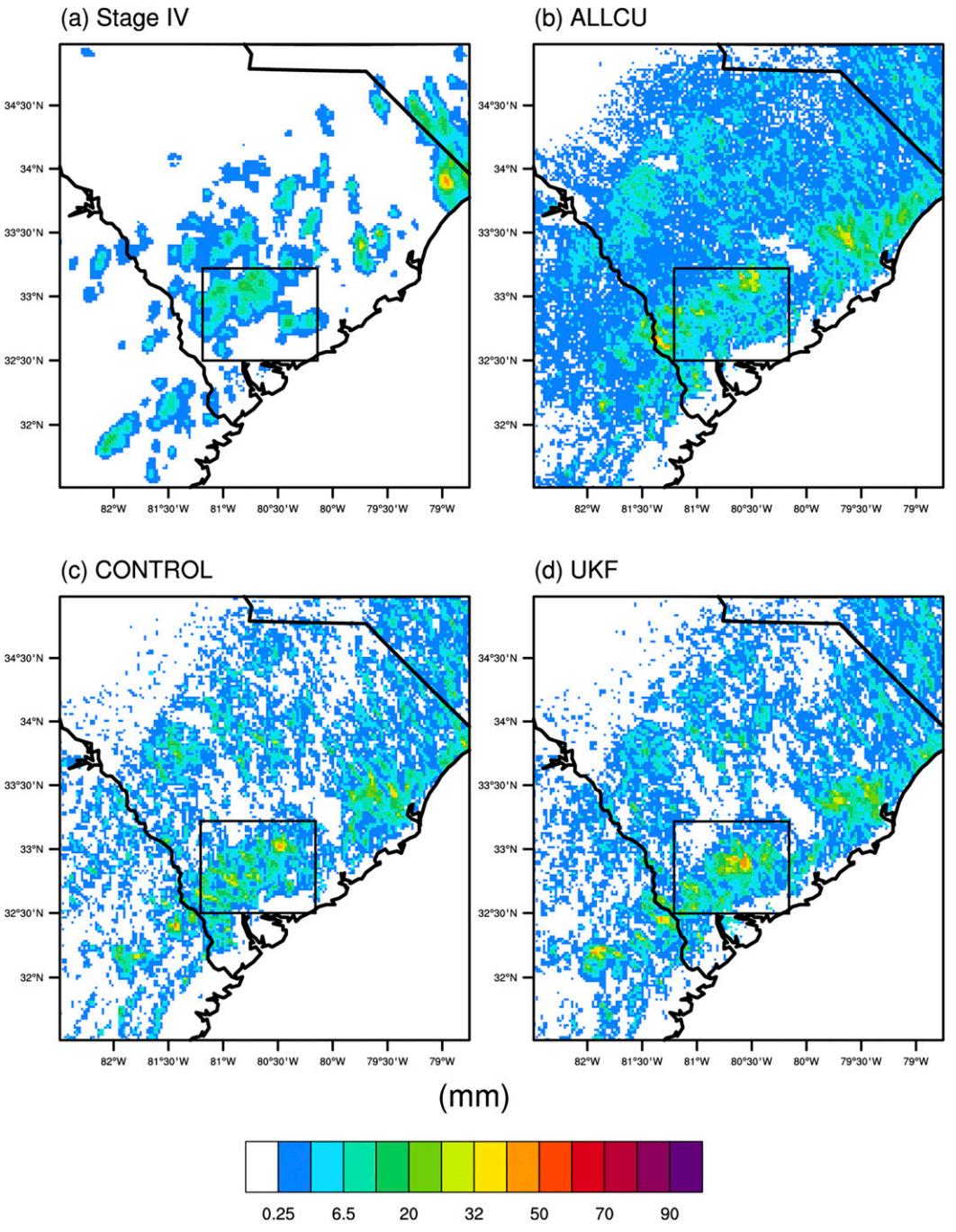

FIG. 10. As in Fig. 8, but for the 1-km domain.

For the intermediate simulation domain, the Stage-IV analyses are regridded to 4 km for comparison to the CONTROL and UKF simulations (Fig. 9a). Differences in the 36-h total simulated precipitation are still apparent at this resolution. Large differences seen in the 12-km domain between the CONTROL and the UKF simulations are not as prominent in the 4-km domain, except for the ALLCU case (Fig. 9b). The ALLCU simulation overpredicts the total precipitation due to excessive precipitation predicted by the original KF cumulus parameterization scheme at high resolutions.

Qualitatively, the CONTROL and the UKF simulations have similar precipitation distributions (Figs. 9c and 9d). A notable difference is a reduction in the light precipitation over the area marked by the black circle (Fig. 9c). Along the coast in southern South Carolina,

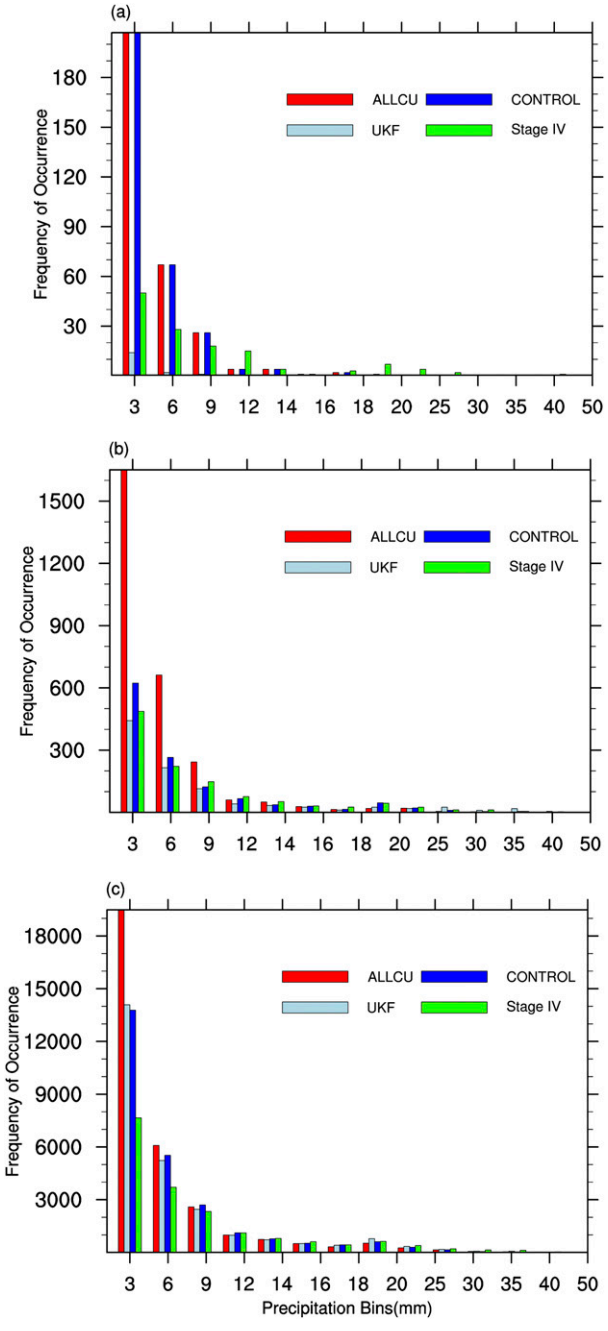

FIG. 11. Histogram of total precipitation for the three simulations and the Stage-IV analyses precipitation amounts over the areal extent of the 1-km domain. Frequency of occurrence for each precipitation bin is shown on the *y* axis, and precipitation amounts for each bin (mm) is shown on the *x* axis. (a) Precipitation amounts for the 12-km domains. (b) Precipitation amounts for the 4-km domains. (c) Precipitation amounts for the 1-km domains.

where the interaction between the sea breeze and the Sandhills front occurs (Sims and Raman 2016), maximum precipitation amounts in the UKF tend to be higher than in the CONTROL. Precipitation amounts in the UKF simulation over this region exceed the values of Stage-IV analyses and the CONTROL simulation predictions. These results are consistent with the stronger UMF and larger amounts of moisture in the air column for the UKF simulation (Figs. 6 and 7). The KF CP modifications reduces the spurious spatial extent of the simulated precipitation while retaining CAPE and moisture in the column allowing additional strong convection to develop downstream. These results are consistent with the study by Raymond and Zeng (2000), who found that increased moisture in a column led to enhanced convection and precipitation. Also, idealized experiments from Derbyshire et al. (2004) found that the lack of midlevel moisture can suppress deep convection.

The improvement in precipitation forecast for the UKF simulation is indicated by the reduced FBIAS in all but one threshold category (Table 2). This reduced FBIAS at most thresholds represents a reduction in simulated precipitation, which is an improvement over the CONTROL simulation. Also, the average precipitation bias (ME) in the UKF simulation is less (1.28 mm) than that in the CONTROL simulation (1.33 mm).

For the innermost domain, the Stage-IV analyses are interpolated to the 1-km domain (Fig. 10a) for direct comparison to the three simulations. The ALLCU simulation generates too much precipitation as expected (Fig. 10b). The precipitation amounts and areal extent are larger than the Stage-IV analyses and the other two simulations: the CONTROL (Fig. 10c) and the UKF (Fig. 10d). Qualitatively, the CONTROL simulation and the UKF simulation exhibit similar precipitation patterns and amounts and are in better agreement than the corresponding coarser domains. This is expected since the UKF CP scheme, although active, is highly attenuated at this resolution. The FBIAS for thresholds between 1.27 and 2.54 mm have comparable values (Table 2). For the highest precipitation threshold exceeding 12.7 mm, both simulations have high FBIAS values indicating over prediction of precipitation. For the UKF simulation, the CP scheme does little to mitigate the prediction of excess precipitation at this resolution. Average ME for the CONTROL and the UKF simulations are 1.3 and 1.45 mm, respectively. Higher precipitation bias in the UKF simulation is likely due to increased intensity of convection suggesting that more intense precipitation results from the UKF modifications, even at 1-km grid spacing.

The distribution of precipitation amounts over the areal extent of the 1-km domain is shown in Fig. 11. At 12 km, the CONTROL and the ALLCU simulations

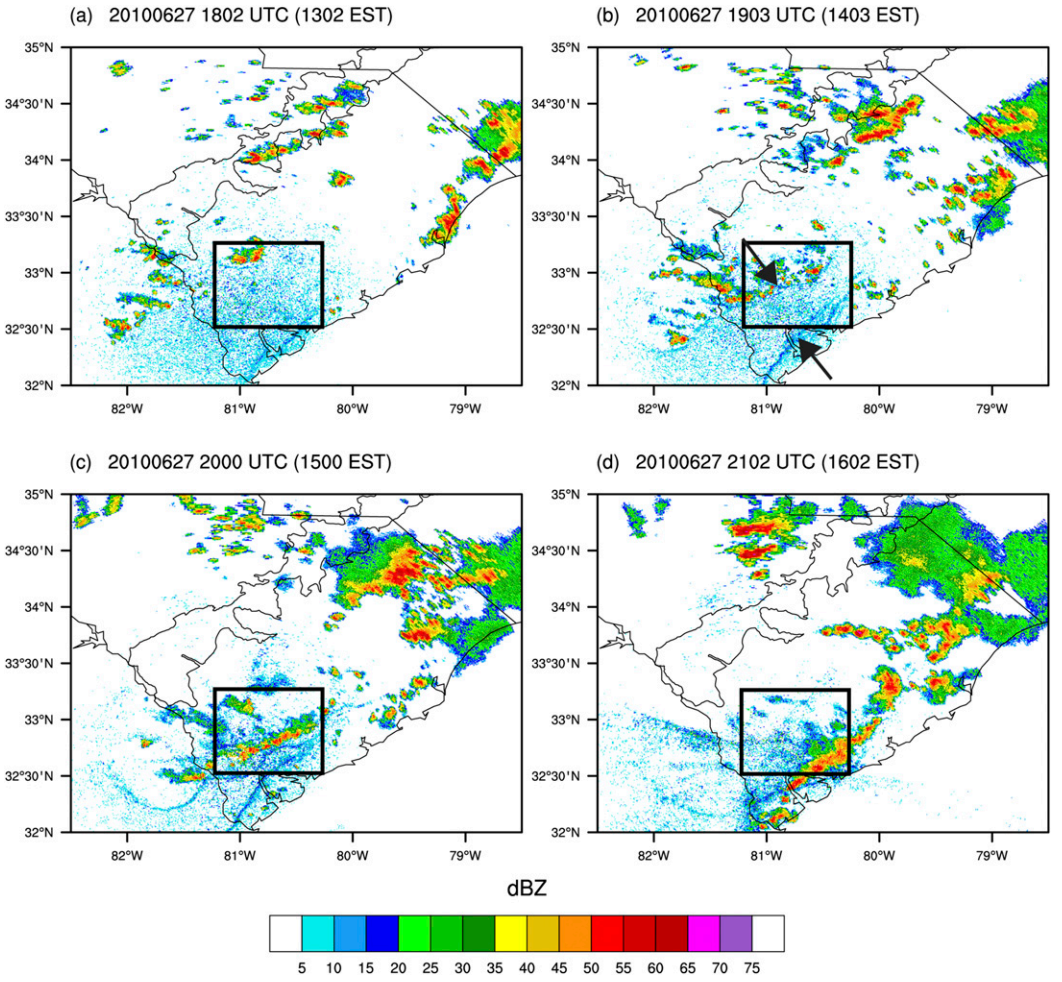

FIG. 12. Snapshots in time of the base-level radar reflectivity (dBZ) from the Doppler radar in Charleston, SC, on 27 Jun 2010. The black box indicates the study area, depicted in Fig. 1. (a) The sea-breeze front is indicated by the thin blue line of reflectivity at 1802 UTC. (b) The development of the outflow from convection in the Sandhills (Sandhills front) and the sea-breeze front are indicated by opposing arrows at 1903 UTC. (c) Merging of the sea-breeze front and the Sandhills front at 2000 UTC. (d) Intense convection over southern SC at 2102 UTC where the two fronts merged.

predict too much light precipitation for amounts between 3 and 6 mm (Fig. 11a). The UKF simulation does not predict precipitation amounts greater than 9 mm in the 12-km domain. At 4 km, the UKF simulation matches the Stage-IV analyses well for amounts less than 9 mm (Fig. 11b). There is a reduction in light precipitation amounts in the UKF simulation. For amounts greater than 9 mm, the CONTROL and UKF simulations predict similar amounts.

For the 1-km domain (Fig. 11c), the distribution of precipitation amounts in the UKF and CONTROL simulations are comparable. Both simulations still produce too much light precipitation (3-mm threshold), but are similar to Stage-IV analyses for amounts greater than 6 mm. It is apparent that there is too much spatial coverage of precipitation at 1 km in both these simulations than in Stage-IV analyses.

5. Case 2 simulations

Another mesoscale interaction event that occurred on 27 June 2010 in the coastal Carolinas is presented as case 2. The timing of the convection and the interaction of the two frontal features is indicated by the radar reflectivity (Fig. 12). At 1802 UTC, radar reflectivity indicates isolated convection occurring near the Sandhills region in South Carolina (Fig. 12a). By 1903 UTC, this convection has intensified and the resulting Sandhills front has moved toward the coast (Fig. 12b). The sea-breeze front is indicated by a thin blue line of radar reflectivity

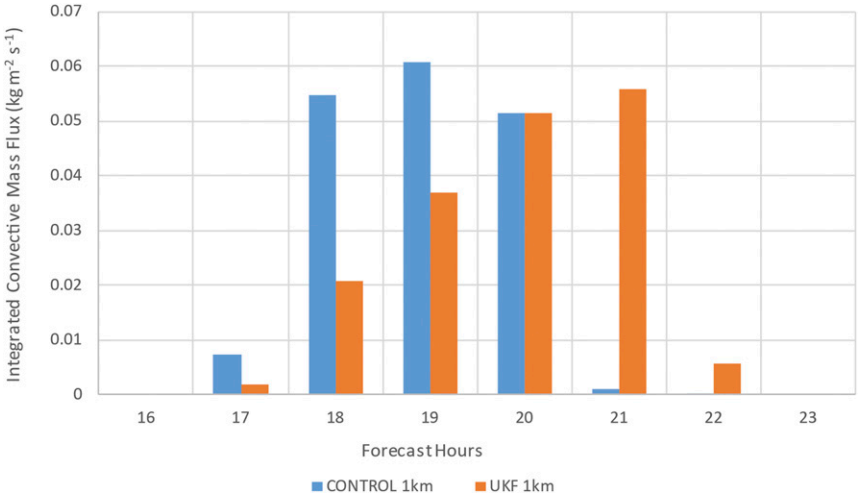

FIG. 13. As in Fig. 6, but during the afternoon of 27 Jun 2010. Forecast hours 16–23 correspond to times 1600 UTC 27 Jun–2300 UTC 27 Jun 2010.

near the coast. At 2000 UTC, the Sandhills front and the sea-breeze front converge (Fig. 12c). By 2102 UTC the two mesoscale frontal features have merged and the consequent deep convection is apparent in the radar reflectivity in Fig. 12d.

Like case 1, two simulations are performed: CONTROL and UKF. The inclusion of subgrid-scale clouds in the UKF CP scheme causes a reduction in incoming radiation in all three domains (not shown). As in case 1, the grid-averaged differences in downward shortwave radiation from the CONTROL are the largest in the 12-km domain with a maximum reduction of 84 W m^{-2}. In the 4- and 1-km domains, the maximum reductions during daytime heating are 21 and 8 W m^{-2}, respectively.

These reductions in radiation also affect the development of convection. The development of convection in the CONTROL and the UKF simulations are apparent in the resolved UMF on 27 June 2010 (Fig. 13). As in case 1, the comparison of the mass flux for case 2 is limited to the area shown by the black box (Fig. 1), the location where the interaction occurred between the two mesoscale fronts. At approximately 1800 UTC 27 June 2010, the UMF magnitude in the CONTROL simulation exceeds that of the UKF simulation (Fig. 13), prematurely developing deep convection. At 2100 UTC, the time of interaction (Fig. 12d), convection in the CONTROL simulation has subsided. The UKF simulation captures the timing of the convection better.

A vertical profile of average water vapor mixing ratio at 2100 UTC in the interaction region is shown in Fig. 14. The UKF CP scheme has larger values of water vapor than the CONTROL simulation indicating more moisture in the column, similar to case 1. The vertical profile of average water vapor mixing ratio indicates an increase of 1–3 g kg^{-1} on each domain in the UKF simulation than in the CONTROL. These differences are likely caused by the timing of the convection, with the UKF simulation being more consistent with the observed radar reflectivity (Fig. 12).

The FBIAS and ME for the simulated precipitation for the 36-h period beginning at 0000 UTC 27 June 2010 is provided in Table 3. For the 12-km domain, the UKF and the CONTROL simulations have similar frequency biases for precipitation thresholds less than 2.54 mm. A dry bias is present in both simulations at

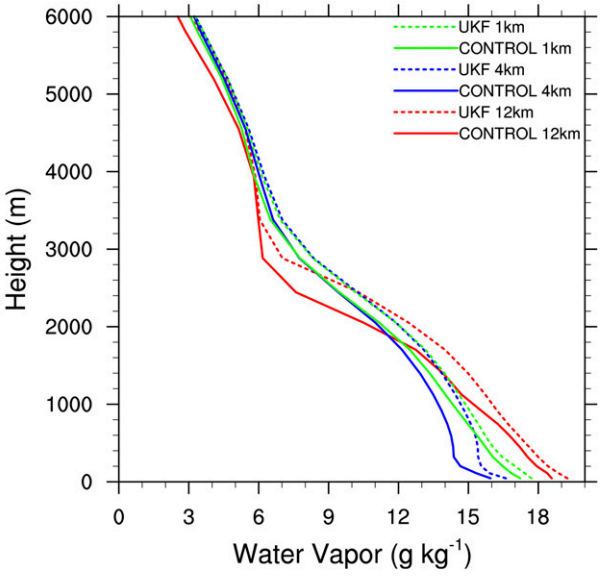

FIG. 14. Vertical profile of average water vapor mixing ratio (g kg^{-1}) in the interaction region for the CONTROL and the UKF simulations for each of the domains at 2100 UTC 27 Jun 2010. Solid (dashed) lines represent the CONTROL (UKF) simulations.

TABLE 3. Frequency bias (FBIAS) and mean error (ME) for total precipitation (mm) for the 27 Jun 2010 case over the South Carolina region for each simulation.

Statistic	Threshold	CONTROL 12 km	UKF 12 km	CONTROL 4 km	UKF 4 km	CONTROL 1 km	UKF 1 km
FBIAS	≥0.254	0.931	0.920	0.679	1.163	0.591	1.092
FBIAS	≥1.270	0.943	0.905	0.623	1.113	0.512	0.978
FBIAS	≥2.540	0.847	0.853	0.631	0.948	0.489	0.895
FBIAS	≥6.350	0.760	0.333	0.709	0.887	0.433	0.758
FBIAS	≥12.700	0.210	0.145	0.655	0.968	0.365	0.559
ME		−4.700	−4.999	−3.640	−0.927	−5.478	−3.511

amounts greater than the 6.35-mm threshold; the UKF and CONTROL simulations have frequency biases of 0.33 and 0.76, respectively. This reduction of precipitation at higher thresholds in the UKF simulation for the 12-km domain is similar to the results for case 1. The magnitudes for the ME for both the CONTROL and the UKF simulations are −4.7 and −4.99 mm, respectively. These large biases can be attributed to both simulations not predicting enough precipitation at higher thresholds.

For the 4-km domain, the UKF simulation is relatively unbiased at all precipitation threshold categories with the FBIAS ranging from 1.16 to 0.89. In contrast, the CONTROL simulation appears to have a dry bias at all thresholds, with the FBIAS ranging from 0.62 to 0.71. In this case, the inclusion of the UKF CP scheme at this resolution results in a more correct frequency of occurrence of precipitation. The ME error analysis shows an average bias of −3.64 and −0.93 mm for the CONTROL and the UKF simulations, respectively.

Additionally, the 1-km domains have similar trends in the biases as the 4-km domains. For amounts greater than 0.254 mm, the CONTROL and UKF simulations have a FBIAS of 0.59 and 1.1, respectively. The UKF simulation is less biased than the CONTROL simulation at all precipitation thresholds. The UKF simulation also has less average bias than the CONTROL with a ME of −3.5 and −5.5 mm, respectively.

Spatial representation of the 36-h precipitation totals for the 1-km domain is shown in Fig. 15a. Stage-IV analyses indicate increased precipitation related to the interaction between the sea-breeze front and the Sandhills front. The black oval encompasses this region of mesoscale interaction. The CONTROL simulation reasonably predicts the spatial pattern of precipitation (Fig. 15b) but misplaces the precipitation maximum associated with the interaction to the southwest. Precipitation amounts along the coast indicate that the UKF simulation (Fig. 15c) captures the location of the maximum better. Neither simulation predicts the large precipitation maxima associated with the sea-breeze front indicated by Stage-IV analyses in northeast South Carolina.

6. Summary and conclusions

Two regional mesoscale features, the sea-breeze front and the Sandhills front, regularly form and interact during summers in the Carolinas. These interactions can initiate convection and are simulated using the WRF Model. These simulations incorporate modifications to the Kain–Fritsch (KF) cumulus parameterization (CP) scheme and are evaluated to assess their impact on mesoscale convection and precipitation patterns.

These modifications, the updated KF (UKF), include adjustments to three aspects of the KF CP scheme: the cloud–radiation interaction, the convective time step, and the entrainment formulation. Radiation is adjusted by the inclusion of subgrid-scale cumulus clouds from the KF CP scheme. Additionally, the time-scale and entrainment formulations incorporate a grid-spacing-aware scaling parameter. This parameter modulates the strength of the convection as a function of the domain grid spacing. The UKF updates presented in this research are now available in the multiscale Kain–Fritsch (MSKF) scheme (Alapaty et al. 2014a).

The modified KF CP scheme reduces the incoming solar radiation in the UKF simulations, thus decreasing the near-surface temperature in areas of deep convection. Also, the timing of convection related to the interaction between the sea-breeze and the Sandhills front is improved in the UKF simulations. These modifications help to mitigate the early development of convection in the CONTROL simulations with the original KF scheme. Further, the longer convective turnover time scale and higher entrainment rates increase the moisture available to the grid-scale microphysics scheme. These changes in the CP scheme result in better timing and increased strength of convection thus providing more realistic precipitation patterns.

At 12 km, the simulation of excessive widespread precipitation is attenuated and there are improvements in the locations of the maximum amounts due to the modified KF

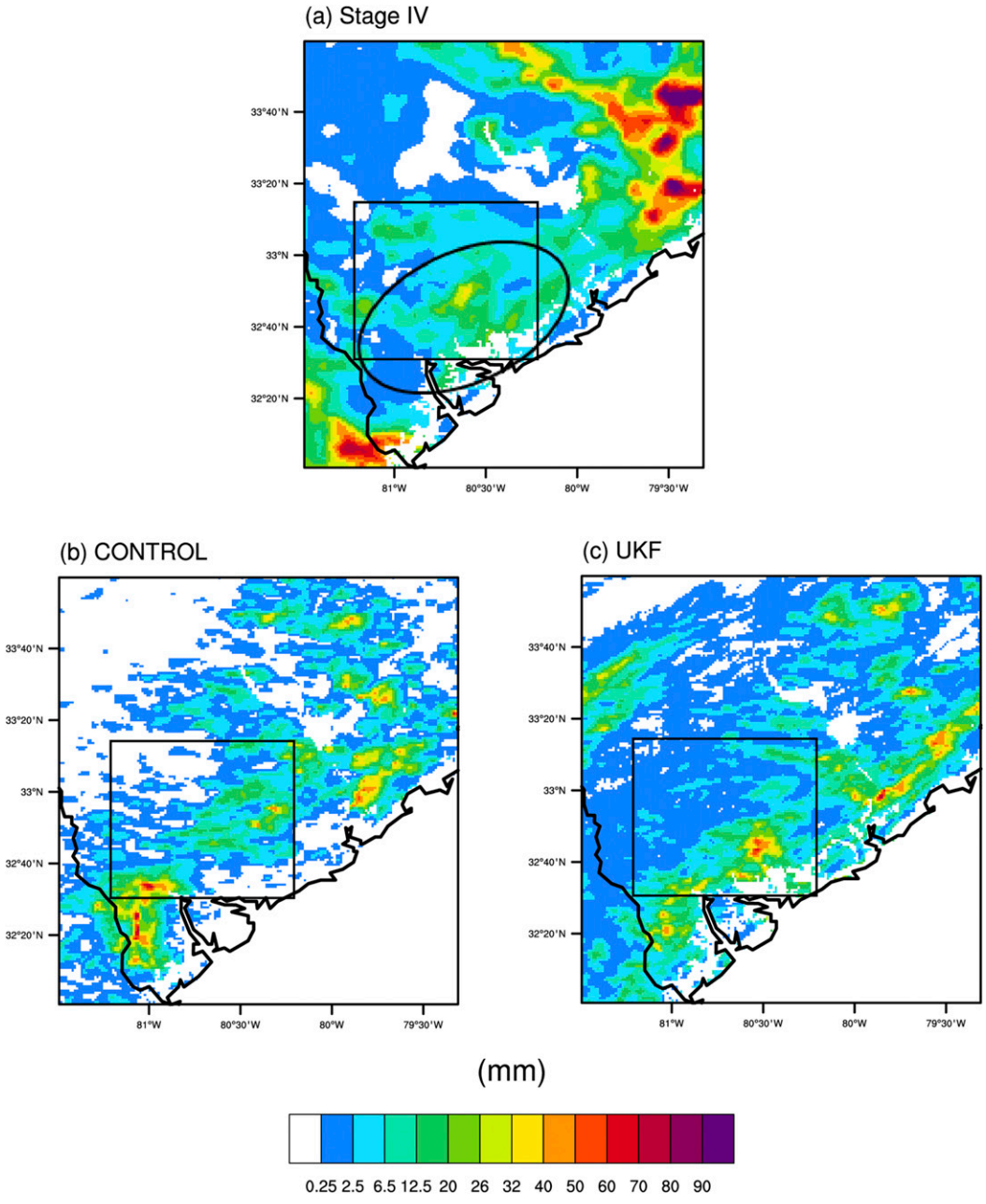

FIG. 15. Total accumulated precipitation (mm) centered over South Carolina for the period 0000 UTC 27 Jun–1200 UTC 28 Jun 2010. The black box indicates the study area, depicted in Fig. 1. (a) Stage-IV analyses regridded to the 1-km WRF domain. Region of precipitation associated with the mesoscale interaction is indicated by the black oval. (b) Predicted precipitation from the 1-km CONTROL simulation. (c) Predicted precipitation from the 1-km UKF simulation.

scheme. Slower activation of the UKF CP scheme reduces the widespread precipitation, thus resulting in the prediction of fewer intense convective cells. This may not correspond to improved accuracy since predicted locations of the simulated and observed precipitation amounts do not always match. Also, the UKF simulation tends to underpredict the precipitation amounts at higher threshold categories. However, the UKF simulations do tend to reduce the average total precipitation biases on most domains in the two cases and the biases are lower at most precipitation thresholds.

Effects of the modified KF CP scheme are stronger in the 12-km domain than in the finer resolutions of the 4- and 1-km domains. These results are to be expected

since the scheme ramps down its impact as grid spacing gets smaller. At 4 km, there is a reduction in spurious light precipitation and an increase in the intensity of convection. At these finer resolutions, the UKF simulations tend to decrease the number of convective cells in regions adjacent to strong convection, producing fewer but stronger convective cells. Even at 1 km, where the updated Kain–Fritsch (UKF) effects are attenuated, there are reduced daytime precipitation frequency biases. However, it is important to note that improvements in the UKF simulations may not be present at all locations and all times.

Acknowledgments. This research was internally supported by the State Climate Office of North Carolina at NCSU and the U.S. EPA's Office of Research and Development under the Air, Climate, and Energy (ACE) Program. Our appreciation goes to Dr. Jerold A. Herwehe of the U.S. EPA for his valuable comments on this work. Also, the authors thank the editor and the anonymous reviewers for their very valuable suggestions in improving this manuscript. This research has been subjected to the U.S. EPA's administrative review and approved for publication. The views expressed and the contents are solely the responsibility of the authors, and do not necessarily represent the official views of the U.S. EPA.

REFERENCES

Alapaty, K., J. A. Herwehe, T. L. Otte, C. G. Nolte, O. R. Bullock, M. S. Mallard, J. S. Kain, and J. Dudhia, 2012: Introducing subgrid-scale cloud feedbacks to radiation for regional meteorological and climate modeling. *Geophys. Res. Lett.*, **39**, L24809, doi:10.1029/2012GL054031.

——, J. S. Kain, J. A. Herwehe, O. R. Bullock Jr., M. S. Mallard, T. L. Spero, and C. G. Nolte, 2014a: Multiscale Kain-Fritsch Scheme: Formulations and tests. *Annual CMAS Conf.*, Chapel Hill, NC, https://www.cmascenter.org/conference/2014/slides/kiran_alapaty_multiscale_kain-fritsch_2014.pptx.

——, ——, ——, ——, Y. Zheng, M. S. Mallard, and A. P. Sims, 2014b: Achieving scale-independent convection representation with the Kain-Fritsch scheme. *15th Annual WRF Users' Workshop*, Boulder, CO, UCAR, P10, http://www2.mmm.ucar.edu/wrf/users/workshops/WS2014/posters/p10.pdf.

Arakawa, A., and C.-M. Wu, 2013: A unified representation of deep moist convection in numerical modeling of the atmosphere. Part I. *J. Atmos. Sci.*, **70**, 1977–1992, doi:10.1175/JAS-D-12-0330.1.

Arya, S. P., 2001: *Introduction to Micrometeorology*. Academic Press, 307 pp.

Bechtold, P., M. Köhler, T. Jung, F. Doblas-Reyes, M. Leutbecher, M. J. Rodwell, F. Vitart, and G. Balsamo, 2008: Advances in simulating atmospheric variability with the ECMWF model: From synoptic to decadal time-scales. *Quart. J. Roy. Meteor. Soc.*, **134**, 1337–1351, doi:10.1002/qj.289.

Blossey, P. N., C. S. Bretherton, J. Cetrone, and M. Kharoutdinov, 2007: Cloud-resolving model simulations of KWAJEX: Model sensitivities and comparisons with satellite and radar observations. *J. Atmos. Sci.*, **64**, 1488–1508, doi:10.1175/JAS3982.1.

Bryan, G. H., and H. Morrison, 2012: Sensitivity of a simulated squall line to horizontal resolution and parameterization of microphysics. *Mon. Wea. Rev.*, **140**, 202–225, doi:10.1175/MWR-D-11-00046.1.

Bullock, R., K. Alapaty, J. A. Herwehe, and J. S. Kain, 2015: A dynamically computed convective time scale for the Kain–Fritsch convective parameterization scheme. *Mon. Wea. Rev.*, **143**, 2105–2120, doi:10.1175/MWR-D-14-00251.1.

Cao, Z., and D.-L. Zhang, 2016: Analysis of missed summer severe rainfall forecasts. *Wea. Forecasting*, **31**, 433–450, doi:10.1175/WAF-D-15-0119.1.

Choi, I.-J., E. K. Jin, J.-Y. Han, S.-Y. Kim, and Y. Kwon, 2015: Sensitivity of diurnal variation in simulated precipitation during East Asian summer monsoon to cumulus parameterization schemes. *J. Geophys. Res. Atmos.*, **120**, 11 971–11 987, doi:10.1002/2015JD023810.

Cintineo, R., J. A. Otkin, M. Xue, and F. Kong, 2014: Evaluating the performance of planetary boundary layer and cloud microphysical parameterization schemes in convection permitting ensemble forecasts using synthetic *GOES-13* satellite observations. *Mon. Wea. Rev.*, **142**, 163–182, doi:10.1175/MWR-D-13-00143.1.

Clark, A. J., W. A. Gallus, and T. C. Chen, 2007: Comparison of the diurnal precipitation cycle in convection-resolving and non-convection-resolving mesoscale models. *Mon. Wea. Rev.*, **135**, 3456–3473, doi:10.1175/MWR3467.1.

——, ——, M. Xue, and F. Y. Kong, 2009: A comparison of precipitation forecast skill between small convection-allowing and large convection-parameterizing ensembles. *Wea. Forecasting*, **24**, 1121–1140, doi:10.1175/2009WAF2222222.1.

Del Genio, A. D., and J. Wu, 2010: The role of entrainment in the diurnal cycle of continental convection. *J. Climate*, **23**, 2722–2738, doi:10.1175/2009JCLI3340.1.

Derbyshire, S. H., I. Beau, P. Bechtold, J.-Y. Grandpeix, J.-M. Piriou, J.-L. Redelsperger, and P. M. M. Soares, 2004: Sensitivity of moist convection to environmental humidity. *Quart. J. Roy. Meteor. Soc.*, **130**, 3055–3079, doi:10.1256/qj.03.130.

Fritsch, J. M., and C. F. Chappell, 1980: Numerical prediction of convectively driven mesoscale pressure systems. Part I: Convective parameterization. *J. Atmos. Sci.*, **37**, 1722–1733, doi:10.1175/1520-0469(1980)037<1722:NPOCDM>2.0.CO;2.

——, and R. E. Carbone, 2004: Improving quantitative precipitation forecasts in the warm season: A USWRP research and development strategy. *Bull. Amer. Meteor. Soc.*, **85**, 955–965, doi:10.1175/BAMS-85-7-955.

——, C. F. Chappell, and L. R. Hoxit, 1976: The use of large-scale budgets for convective parameterization. *Mon. Wea. Rev.*, **104**, 1408–1418, doi:10.1175/1520-0493(1976)104<1408:TUOLSB>2.0.CO;2.

Gilleland, E., D. Ahijevych, B. G. Brown, B. Casati, and E. E. Ebert, 2009: Intercomparison of spatial forecast verification methods. *Wea. Forecasting*, **24**, 1416–1430, doi:10.1175/2009WAF2222269.1.

Grant, A. L. M., and A. P. Lock, 2004: The turbulent kinetic energy budget for shallow cumulus convection. *Quart. J. Roy. Meteor. Soc.*, **130**, 401–422, doi:10.1256/qj.03.50.

Habib, E., B. F. Larson, and J. Graschel, 2009: Validation of NEXRAD multisensory precipitation estimates using an experimental dense rain gauge network in south Louisiana. *J. Hydrol.*, **373**, 463–478, doi:10.1016/j.jhydrol.2009.05.010.

Herwehe, J. A., K. Alapaty, T. L. Spero, and C. G. Nolte, 2014a: Increasing the credibility of regional climate simulations by

introducing subgrid-scale cloud-radiation interactions. *J. Geophys. Res. Atmos.*, **119**, 5317–5330, doi:10.1002/2014JD021504.

——, ——, J. S. Kain, and R. Bullock Jr., 2014b: Summer season evaluation of a new multiscale Kain-Fritsch convective parameterization. *15th Annual WRF Users' Workshop*, Boulder, CO, UCAR, P11, http://www2.mmm.ucar.edu/wrf/users/workshops/WS2014/posters/p11.pdf.

Iacono, M. J., J. S. Delamere, E. J. Mlawer, M. W. Shephard, S. A. Clough, and W. D. Collins, 2008: Radiative forcing by long-lived greenhouse gases: Calculations with the AER radiative transfer models. *J. Geophys. Res.*, **113**, D13103, doi:10.1029/2008JD009944.

Janowiak, J. E., V. J. Dagostaro, V. E. Kousky, and R. J. Joyce, 2007: An examination of precipitation in observations and model forecasts during NAME with emphasis on the diurnal cycle. *J. Climate*, **20**, 1680–1692, doi:10.1175/JCLI4084.1.

Kain, J. S., 2004: The Kain–Fritsch convective parameterization: An update. *J. Appl. Meteor.*, **43**, 170–181, doi:10.1175/1520-0450(2004)043<0170:TKCPAU>2.0.CO;2.

——, and J. M. Fritsch, 1990: A one-dimensional entraining/detraining plume model and its application in convective parameterization. *J. Atmos. Sci.*, **47**, 2784–2802, doi:10.1175/1520-0469(1990)047<2784:AODEPM>2.0.CO;2.

——, and ——, 1993: Convective parameterization for mesoscale models: The Kain–Fritsch scheme. *The Representation of Cumulus Convection in Numerical Models*, *Meteor. Monogr.*, No. 46, Amer. Meteor. Soc., 165–170.

Kim, D., and Coauthors, 2009: Application of MJO simulation diagnostics to climate models. *J. Climate*, **22**, 6413–6436, doi:10.1175/2009JCLI3063.1.

Lee, M.-I., and Coauthors, 2007: An analysis of the warm-season diurnal cycle over the continental United States and northern Mexico in general circulation models. *J. Hydrometeor.*, **8**, 344–366, doi:10.1175/JHM581.1.

Liang, X.-Z., L. Li, A. Dai, and K. E. Kunkel, 2004: Regional climate model simulation of summer precipitation diurnal cycle over the United States. *Geophys. Res. Lett.*, **31**, L24208, doi:10.1029/2004GL021054.

Lin, Y., and K. E. Mitchell, 2005: The NCEP Stage II/IV hourly precipitation analyses: Development and applications. *19th Conf. on Hydrology*, San Diego, CA, Amer. Meteor. Soc., 1.2, https://ams.confex.com/ams/Annual2005/techprogram/paper_83847.htm.

——, M. Zhao, Y. Ming, J.-C. Golaz, L. J. Donner, S. A. Klein, V. Ramaswamy, and S. Xie, 2013: Precipitation partitioning, tropical clouds, and intraseasonal variability in GFDL AM2. *J. Climate*, **26**, 5453–5466, doi:10.1175/JCLI-D-12-00442.1.

Liu, C.-H., M. W. Moncrieff, J. D. Tuttle, and R. E. Carbone, 2006: Explicit and parameterized episodes of warm-season precipitation over the continental United States. *Adv. Atmos. Sci.*, **23**, 91–105, doi:10.1007/s00376-006-0010-9.

Raman, S., A. Sims, R. Ellis, and R. Boyles, 2005: Numerical simulation of mesoscale circulations in a region of contrasting soil types. *Pure Appl. Geophys.*, **162**, 1689–1714, doi:10.1007/s00024-005-2689-4.

Raymond, D. J., and X. Zeng, 2000: Instability and large-scale circulations in a two-column model of the tropical troposphere. *Quart. J. Roy. Meteor. Soc.*, **126**, 3117–3135, doi:10.1002/qj.49712657007.

Robe, F. R., and K. A. Emanuel, 1996: Moist convective scaling: Some inferences from three-dimensional cloud ensemble simulations. *J. Atmos. Sci.*, **53**, 3265–3275, doi:10.1175/1520-0469(1996)053<3265:MCSSIF>2.0.CO;2.

Romps, D. M., and Z. Kuang, 2010: Nature versus nurture in shallow convection. *J. Atmos. Sci.*, **67**, 1655–1666, doi:10.1175/2009JAS3307.1.

Sims, A. P., and S. Raman, 2016: Interaction between two distinct mesoscale circulations during summer in the coastal region of eastern USA. *Bound.-Layer Meteor.*, **160**, 113–132, doi:10.1007/s10546-015-0125-6.

Skamarock, W. C., and J. B. Klemp, 2008: A time-split nonhydrostatic atmospheric model for weather and forecasting applications. *J. Comput. Phys.*, **227**, 3465–3485, doi:10.1016/j.jcp.2007.01.037.

Stevens, D. E., and C. S. Bretherton, 1999: Effects of resolution on the simulation of stratocumulus entrainment. *Quart. J. Roy. Meteor. Soc.*, **125**, 425–439, doi:10.1002/qj.49712555403.

Tokioka, T., K. Yamazaki, A. Kitoh, and T. Ose, 1988: The equatorial 30-60 day oscillation and the Arakawa-Schubert penetrative cumulus parameterization. *J. Meteor. Soc. Japan*, **66**, 883–901, doi:10.2151/jmsj1965.66.6_883.

Wang, S., and A. H. Sobel, 2011: Response of convection to relative sea surface temperature: Cloud-resolving simulations in two and three dimensions. *J. Geophys. Res.*, **116**, D11119, doi:10.1029/2010JD015347.

Wang, W., and N. L. Seaman, 1997: A comparison study of convective parameterization schemes in a mesoscale model. *Mon. Wea. Rev.*, **125**, 252–278, doi:10.1175/1520-0493(1997)125<0252:ACSOCP>2.0.CO;2.

Weisman, M. L., W. C. Skamarock, and J. B. Klemp, 1997: The resolution dependence of explicitly modeled convective systems. *Mon. Wea. Rev.*, **125**, 527–548, doi:10.1175/1520-0493(1997)125<0527:TRDOEM>2.0.CO;2.

Wootten, A., and R. P. Boyles, 2014: Comparison of NCEP multisensor precipitation estimates with independent gauge data over the eastern United States. *J. Appl. Meteor. Climatol.*, **53**, 2848–2862, doi:10.1175/JAMC-D-14-0034.1.

Xu, K.-M., and S. K. Krueger, 1991: Evaluation of cloudiness parameterizations using a cumulus ensemble model. *Mon. Wea. Rev.*, **119**, 342–367, doi:10.1175/1520-0493(1991)119<0342:EOCPUA>2.0.CO;2.

Yu, X., and T.-Y. Lee, 2010: Role of convective parameterization in simulations of a convection band at grey-zone resolutions. *Tellus*, **62A**, 617–632, doi:10.1111/j.1600-0870.2010.00470.x.

Zheng, Y., K. Alapaty, J. Herwehe, A. Del Genio, and D. Niyogi, 2016: improving high-resolution weather forecasts using the Weather Research and Forecasting (WRF) Model with an updated Kain–Fritsch scheme. *Mon. Wea. Rev.*, **144**, 833–860, doi:10.1175/MWR-D-15-0005.1.